Measurement of the $B^+ \to \omega l^+ \nu$ and $B^+ \to \eta l^+ \nu$ branching fractions

B. Aubert,[1] M. Bona,[1] Y. Karyotakis,[1] J. P. Lees,[1] V. Poireau,[1] E. Prencipe,[1] X. Prudent,[1] V. Tisserand,[1] J. Garra Tico,[2] E. Grauges,[2] L. Lopez,[3a,3b] A. Palano,[3a,3b] M. Pappagallo,[3a,3b] G. Eigen,[4] B. Stugu,[4] L. Sun,[4] G. S. Abrams,[5] M. Battaglia,[5] D. N. Brown,[5] R. N. Cahn,[5] R. G. Jacobsen,[5] L. T. Kerth,[5] Yu. G. Kolomensky,[5] G. Lynch,[5] I. L. Osipenkov,[5] M. T. Ronan,[5,*] K. Tackmann,[5] T. Tanabe,[5] C. M. Hawkes,[6] N. Soni,[6] A. T. Watson,[6] H. Koch,[1] T. Schroeder,[1] D. Walker,[8] D. J. Asgeirsson,[9] B. G. Fulsom,[9] C. Hearty,[9] T. S. Mattison,[9] J. A. McKenna,[9] M. Barrett,[10] A. Khan,[10] V. E. Blinov,[11] A. D. Bukin,[11] A. R. Buzykaev,[11] V. P. Druzhinin,[11] V. B. Golubev,[11] A. P. Onuchin,[11] S. I. Serednyakov,[11] Yu. I. Skovpen,[11] E. P. Solodov,[11] K. Yu. Todyshev,[11] M. Bondioli,[12] S. Curry,[12] I. Eschrich,[12] D. Kirkby,[12] A. J. Lankford,[12] P. Lund,[12] M. Mandelkern,[12] E. C. Martin,[12] D. P. Stoker,[12] S. Abachi,[13] C. Buchanan,[13] J. W. Gary,[14] F. Liu,[14] O. Long,[14] B. C. Shen,[14,*] G. M. Vitug,[14] Z. Yasin,[14] L. Zhang,[14] V. Sharma,[15] C. Campagnari,[16] T. M. Hong,[16] D. Kovalskyi,[16] M. A. Mazur,[16] J. D. Richman,[16] T. W. Beck,[17] A. M. Eisner,[17] C. J. Flacco,[17] C. A. Heusch,[17] J. Kroseberg,[17] W. S. Lockman,[17] A. J. Martinez,[17] T. Schalk,[17] B. A. Schumm,[17] A. Seiden,[17] M. G. Wilson,[17] L. O. Winstrom,[17] C. H. Cheng,[18] D. A. Doll,[18] B. Echenard,[18] F. Fang,[18] D. G. Hitlin,[18] I. Narsky,[18] T. Piatenko,[18] F. C. Porter,[18] R. Andreassen,[19] G. Mancinelli,[19] B. T. Meadows,[19] K. Mishra,[19] M. D. Sokoloff,[19] P. C. Bloom,[20] W. T. Ford,[20] A. Gaz,[20] J. F. Hirschauer,[20] M. Nagel,[20] U. Nauenberg,[20] J. G. Smith,[20] K. A. Ulmer,[20] S. R. Wagner,[20] R. Ayad,[21,†] A. Soffer,[21,‡] W. H. Toki,[21] R. J. Wilson,[21] D. D. Altenburg,[22] E. Feltresi,[22] A. Hauke,[22] H. Jasper,[22] M. Karbach,[22] J. Merkel,[22] A. Petzold,[22] B. Spaan,[22] K. Wacker,[22] M. J. Kobel,[23] W. F. Mader,[23] R. Nogowski,[23] K. R. Schubert,[23] R. Schwierz,[23] A. Volk,[23] D. Bernard,[24] G. R. Bonneaud,[24] E. Latour,[24] M. Verderi,[24] P. J. Clark,[25] S. Playfer,[25] J. E. Watson,[25] M. Andreotti,[26a,26b] D. Bettoni,[26a] C. Bozzi,[26a] R. Calabrese,[26a,26b] A. Cecchi,[26a,26b] G. Cibinetto,[26a,26b] P. Franchini,[26a,26b] E. Luppi,[26a,26b] M. Negrini,[26a,26b] A. Petrella,[26a,26b] L. Piemontese,[26a] V. Santoro,[26a,26b] R. Baldini-Ferroli,[27] A. Calcaterra,[27] R. de Sangro,[27] G. Finocchiaro,[27] S. Pacetti,[27] P. Patteri,[27] I. M. Peruzzi,[27,§] M. Piccolo,[27] M. Rama,[27] A. Zallo,[27] A. Buzzo,[28a] R. Contri,[28a,28b] M. Lo Vetere,[28a,28b] M. M. Macri,[28a] M. R. Monge,[28a,28b] S. Passaggio,[28a] C. Patrignani,[28a,28b] E. Robutti,[28a] A. Santroni,[28a,28b] S. Tosi,[28a,28b] K. S. Chaisanguanthum,[29] M. Morii,[29] A. Adametz,[30] C. Anders,[30] C. Langenbruch,[30] J. Marks,[30] S. Schenk,[30] U. Uwer,[30] V. Klose,[31] H. M. Lacker,[31] D. J. Bard,[32] P. D. Dauncey,[32] J. A. Nash,[32] M. Tibbetts,[32] P. K. Behera,[33] X. Chai,[33] M. J. Charles,[33] U. Mallik,[33] J. Cochran,[34] H. B. Crawley,[34] L. Dong,[34] W. T. Meyer,[34] S. Prell,[34] E. I. Rosenberg,[34] A. E. Rubin,[34] Y. Y. Gao,[35] A. V. Gritsan,[35] Z. J. Guo,[35] C. K. Lae,[35] N. Arnaud,[36] J. Béquilleux,[36] A. D'Orazio,[36] M. Davier,[36] J. Firmino da Costa,[36] G. Grosdidier,[36] A. Höcker,[36] V. Lepeltier,[36] F. Le Diberder,[36] A. M. Lutz,[36] S. Pruvot,[36] P. Roudeau,[36] M. H. Schune,[36] J. Serrano,[36] V. Sordini,[36,‖] A. Stocchi,[36] G. Wormser,[36] D. J. Lange,[37] D. M. Wright,[37] I. Bingham,[38] J. P. Burke,[38] C. A. Chavez,[38] J. R. Fry,[38] E. Gabathuler,[38] R. Gamet,[38] D. E. Hutchcroft,[38] D. J. Payne,[38] C. Touramanis,[38] A. J. Bevan,[39] C. K. Clarke,[39] K. A. George,[39] F. Di Lodovico,[39] R. Sacco,[39] M. Sigamani,[40] G. Cowan,[40] H. U. Flaecher,[40] D. A. Hopkins,[40] S. Paramesvaran,[40] F. Salvatore,[40] A. C. Wren,[40] D. N. Brown,[41] C. L. Davis,[41] A. G. Denig,[42] M. Fritsch,[42] W. Gradl,[42] G. Schott,[42] K. E. Alwyn,[43] D. Bailey,[43] R. J. Barlow,[43] Y. M. Chia,[43] C. L. Edgar,[43] G. Jackson,[43] G. D. Lafferty,[43] T. J. West,[43] J. I. Yi,[43] J. Anderson,[44] C. Chen,[44] A. Jawahery,[44] D. A. Roberts,[44] G. Simi,[44] J. M. Tuggle,[44] C. Dallapiccola,[45] X. Li,[45] E. Salvati,[45] S. Saremi,[45] R. Cowan,[46] D. Dujmic,[46] P. H. Fisher,[46] G. Sciolla,[46] M. Spitznagel,[46] F. Taylor,[46] R. K. Yamamoto,[46] M. Zhao,[46] P. M. Patel,[47] S. H. Robertson,[47] A. Lazzaro,[48a,48b] V. Lombardo,[48a] F. Palombo,[48a,48b] J. M. Bauer,[49] L. Cremaldi,[49] R. Godang,[49,¶] R. Kroeger,[49] D. A. Sanders,[49] D. J. Summers,[49] H. W. Zhao,[49] M. Simard,[50] P. Taras,[50] F. B. Viaud,[50] H. Nicholson,[51] G. De Nardo,[52a,52b] L. Lista,[52a] D. Monorchio,[52a,52b] G. Onorato,[52a,52b] C. Sciacca,[52a,52b] G. Raven,[53] H. L. Snoek,[53] C. P. Jessop,[54] K. J. Knoepfel,[54] J. M. LoSecco,[54] W. F. Wang,[54] G. Benelli,[55] L. A. Corwin,[55] K. Honscheid,[55] H. Kagan,[55] R. Kass,[55] J. P. Morris,[55] A. M. Rahimi,[55] J. J. Regensburger,[55] S. J. Sekula,[55] Q. K. Wong,[55] N. L. Blount,[56] J. Brau,[56] R. Frey,[56] O. Igonkina,[56] J. A. Kolb,[56] M. Lu,[56] R. Rahmat,[56] N. B. Sinev,[56] D. Strom,[56] J. Strube,[56] E. Torrence,[56] G. Castelli,[57a,57b] N. Gagliardi,[57a,57b] M. Margoni,[57a,57b] M. Morandin,[57a] M. Posocco,[57a] M. Rotondo,[57a] F. Simonetto,[57a,57b] R. Stroili,[57a,57b] C. Voci,[57a,57b] P. del Amo Sanchez,[58] E. Ben-Haim,[58] H. Briand,[58] G. Calderini,[58] J. Chauveau,[58] P. David,[58] L. Del Buono,[58] O. Hamon,[58] Ph. Leruste,[58] J. Ocariz,[58] A. Perez,[58] J. Prendki,[58] S. Sitt,[58] L. Gladney,[59] M. Biasini,[60a,60b] R. Covarelli,[60a,60b] E. Manoni,[60a,60b] C. Angelini,[61a,61b] G. Batignani,[61a,61b] S. Bettarini,[61a,61b] M. Carpinelli,[61a,61b,**] A. Cervelli,[61a,61b] F. Forti,[61a,61b] M. A. Giorgi,[61a,61b] A. Lusiani,[61a,61c] G. Marchiori,[61a,61b] M. Morganti,[61a,61b] N. Neri,[61a,61b] E. Paoloni,[61a,61b] G. Rizzo,[61a,61b] J. J. Walsh,[61a] D. Lopes Pegna,[62] C. Lu,[62] J. Olsen,[62] A. J. S. Smith,[62] A. V. Telnov,[62] F. Anulli,[63a] E. Baracchini,[63a,63b] G. Cavoto,[63a] D. del Re,[63a,63b] E. Di Marco,[63a,63b] R. Faccini,[63a,63b] F. Ferrarotto,[63a] F. Ferroni,[63a,63b] M. Gaspero,[63a,63b] P. D. Jackson,[63a] L. Li Gioi,[63a]

M. A. Mazzoni,[63a] S. Morganti,[63a] G. Piredda,[63a] F. Polci,[63a,63b] F. Renga,[63a,63b] C. Voena,[63a] M. Ebert,[64] T. Hartmann,[64] H. Schröder,[64] R. Waldi,[64] T. Adye,[65] B. Franek,[65] E. O. Olaiya,[65] F. F. Wilson,[65] S. Emery,[66] M. Escalier,[66] L. Esteve,[66] S. F. Ganzhur,[66] G. Hamel de Monchenault,[66] W. Kozanecki,[66] G. Vasseur,[66] Ch. Yèche,[66] M. Zito,[66] X. R. Chen,[67] H. Liu,[67] W. Park,[67] M. V. Purohit,[67] R. M. White,[67] J. R. Wilson,[67] M. T. Allen,[68] D. Aston,[68] R. Bartoldus,[68] P. Bechtle,[68] J. F. Benitez,[68] R. Cenci,[68] J. P. Coleman,[68] M. R. Convery,[68] J. C. Dingfelder,[68] J. Dorfan,[68] G. P. Dubois-Felsmann,[68] W. Dunwoodie,[68] R. C. Field,[68] A. M. Gabareen,[68] S. J. Gowdy,[68] M. T. Graham,[68] P. Grenier,[68] C. Hast,[68] W. R. Innes,[68] J. Kaminski,[68] M. H. Kelsey,[68] H. Kim,[68] P. Kim,[68] M. L. Kocian,[68] D. W. G. S. Leith,[68] S. Li,[68] B. Lindquist,[68] S. Luitz,[68] V. Luth,[68] H. L. Lynch,[68] D. B. MacFarlane,[68] H. Marsiske,[68] R. Messner,[68] D. R. Muller,[68] H. Neal,[68] S. Nelson,[68] C. P. O'Grady,[68] I. Ofte,[68] A. Perazzo,[68] M. Perl,[68] B. N. Ratcliff,[68] A. Roodman,[68] A. A. Salnikov,[68] R. H. Schindler,[68] J. Schwiening,[68] A. Snyder,[68] D. Su,[68] M. K. Sullivan,[68] K. Suzuki,[68] S. K. Swain,[68] J. M. Thompson,[68] J. Va'vra,[68] A. P. Wagner,[68] M. Weaver,[68] C. A. West,[68] W. J. Wisniewski,[68] M. Wittgen,[68] D. H. Wright,[68] H. W. Wulsin,[68] A. K. Yarritu,[68] K. Yi,[68] C. C. Young,[68] V. Ziegler,[68] P. R. Burchat,[69] A. J. Edwards,[69] S. A. Majewski,[69] T. S. Miyashita,[69] B. A. Petersen,[69] L. Wilden,[69] S. Ahmed,[70] M. S. Alam,[70] J. A. Ernst,[70] B. Pan,[70] M. A. Saeed,[70] S. B. Zain,[70] S. M. Spanier,[71] B. J. Wogsland,[71] R. Eckmann,[72] J. L. Ritchie,[72] A. M. Ruland,[72] C. J. Schilling,[72] R. F. Schwitters,[72] B. W. Drummond,[73] J. M. Izen,[73] X. C. Lou,[73] F. Bianchi,[74a,74b] D. Gamba,[74a,74b] M. Pelliccioni,[74a,74b] M. Bomben,[75a,75b] L. Bosisio,[75a,75b] C. Cartaro,[75a,75b] G. Della Ricca,[75a,75b] L. Lanceri,[75a,75b] L. Vitale,[75a,75b] V. Azzolini,[76] N. Lopez-March,[76] F. Martinez-Vidal,[76] D. A. Milanes,[76] A. Oyanguren,[76] J. Albert,[77] Sw. Banerjee,[77] B. Bhuyan,[77] H. H. F. Choi,[77] K. Hamano,[77] R. Kowalewski,[77] M. J. Lewczuk,[77] I. M. Nugent,[77] J. M. Roney,[77] R. J. Sobie,[77] T. J. Gershon,[78] P. F. Harrison,[78] J. Ilic,[78] T. E. Latham,[78] G. B. Mohanty,[78] H. R. Band,[79] X. Chen,[79] S. Dasu,[79] K. T. Flood,[79] Y. Pan,[79] M. Pierini,[79] R. Prepost,[79] C. O. Vuosalo,[79] and S. L. Wu[79]

(The *BABAR* Collaboration)

[1]*Laboratoire de Physique des Particules, IN2P3/CNRS et Université de Savoie, F-74941 Annecy-Le-Vieux, France*
[2]*Universitat de Barcelona, Facultat de Fisica, Departament ECM, E-08028 Barcelona, Spain*
[3a]*INFN Sezione di Bari, I-70126 Bari, Italy*
[3b]*Dipartmento di Fisica, Università di Bari, I-70126 Bari, Italy*
[4]*University of Bergen, Institute of Physics, N-5007 Bergen, Norway*
[5]*Lawrence Berkeley National Laboratory and University of California, Berkeley, California 94720, USA*
[6]*University of Birmingham, Birmingham, B15 2TT, United Kingdom*
[1]*Ruhr Universität Bochum, Institut für Experimentalphysik 1, D-44780 Bochum, Germany*
[8]*University of Bristol, Bristol BS8 1TL, United Kingdom*
[9]*University of British Columbia, Vancouver, British Columbia, Canada V6T 1Z1*
[10]*Brunel University, Uxbridge, Middlesex UB8 3PH, United Kingdom*
[11]*Budker Institute of Nuclear Physics, Novosibirsk 630090, Russia*
[12]*University of California at Irvine, Irvine, California 92697, USA*
[13]*University of California at Los Angeles, Los Angeles, California 90024, USA*
[14]*University of California at Riverside, Riverside, California 92521, USA*
[15]*University of California at San Diego, La Jolla, California 92093, USA*
[16]*University of California at Santa Barbara, Santa Barbara, California 93106, USA*
[17]*University of California at Santa Cruz, Institute for Particle Physics, Santa Cruz, California 95064, USA*
[18]*California Institute of Technology, Pasadena, California 91125, USA*
[19]*University of Cincinnati, Cincinnati, Ohio 45221, USA*
[20]*University of Colorado, Boulder, Colorado 80309, USA*
[21]*Colorado State University, Fort Collins, Colorado 80523, USA*
[22]*Technische Universität Dortmund, Fakultät Physik, D-44221 Dortmund, Germany*
[23]*Technische Universität Dresden, Institut für Kernund Teilchenphysik, D-01062 Dresden, Germany*
[24]*Laboratoire Leprince-Ringuet, CNRS/IN2P3, Ecole Polytechnique, F-91128 Palaiseau, France*
[25]*University of Edinburgh, Edinburgh EH9 3JZ, United Kingdom*
[26a]*INFN Sezione di Ferrara, I-44100 Ferrara, Italy*
[26b]*Dipartimento di Fisica, Università di Ferrara, I-44100 Ferrara, Italy*
[27]*INFN Laboratori Nazionali di Frascati, I-00044 Frascati, Italy*
[28a]*INFN Sezione di Genova, I-16146 Genova, Italy*
[28b]*Dipartimento di Fisica, Università di Genova, I-16146 Genova, Italy*
[29]*Harvard University, Cambridge, Massachusetts 02138, USA*
[30]*Universität Heidelberg, Physikalisches Institut, Philosophenweg 12, D-69120 Heidelberg, Germany*

[31]*Humboldt-Universität zu Berlin, Institut für Physik, Newtonstr. 15, D-12489 Berlin, Germany*
[32]*Imperial College London, London, SW7 2AZ, United Kingdom*
[33]*University of Iowa, Iowa City, Iowa 52242, USA*
[34]*Iowa State University, Ames, Iowa 50011-3160, USA*
[35]*Johns Hopkins University, Baltimore, Maryland 21218, USA*
[36]*Laboratoire de l'Accélérateur Linéaire, IN2P3/CNRS et Université Paris-Sud 11, Centre Scientifique d'Orsay, B. P. 34, F-91898 Orsay Cedex, France*
[37]*Lawrence Livermore National Laboratory, Livermore, California 94550, USA*
[38]*University of Liverpool, Liverpool L69 7ZE, United Kingdom*
[39]*Queen Mary, University of London, London, E1 4NS, United Kingdom*
[40]*University of London, Royal Holloway and Bedford New College, Egham, Surrey TW20 0EX, United Kingdom*
[41]*University of Louisville, Louisville, Kentucky 40292, USA*
[42]*Johannes Gutenberg-Universität Mainz, Institut für Kernphysik, D-55099 Mainz, Germany*
[43]*University of Manchester, Manchester M13 9PL, United Kingdom*
[44]*University of Maryland, College Park, Maryland 20742, USA*
[45]*University of Massachusetts, Amherst, Massachusetts 01003, USA*
[46]*Massachusetts Institute of Technology, Laboratory for Nuclear Science, Cambridge, Massachusetts 02139, USA*
[47]*McGill University, Montréal, Québec, Canada H3A 2T8*
[48a]*INFN Sezione di Milano, I-20133 Milano, Italy*
[48b]*Dipartimento di Fisica, Università di Milano, I-20133 Milano, Italy*
[49]*University of Mississippi, University, Mississippi 38677, USA*
[50]*Université de Montréal, Physique des Particules, Montréal, Québec, Canada H3C 3J7*
[51]*Mount Holyoke College, South Hadley, Massachusetts 01075, USA*
[52a]*INFN Sezione di Napoli, I-80126 Napoli, Italy*
[52b]*Dipartimento di Scienze Fisiche, Università di Napoli Federico II, I-80126 Napoli, Italy*
[53]*NIKHEF, National Institute for Nuclear Physics and High Energy Physics, NL-1009 DB Amsterdam, The Netherlands*
[54]*University of Notre Dame, Notre Dame, Indiana 46556, USA*
[55]*Ohio State University, Columbus, Ohio 43210, USA*
[56]*University of Oregon, Eugene, Oregon 97403, USA*
[57a]*INFN Sezione di Padova, I-35131 Padova, Italy*
[57b]*Dipartimento di Fisica, Università di Padova, I-35131 Padova, Italy*
[58]*Laboratoire de Physique Nucléaire et de Hautes Energies, IN2P3/CNRS, Université Pierre et Marie Curie-Paris6, Université Denis Diderot-Paris7, F-75252 Paris, France*
[59]*University of Pennsylvania, Philadelphia, Pennsylvania 19104, USA*
[60a]*INFN Sezione di Perugia, I-06100 Perugia, Italy*
[60b]*Dipartimento di Fisica, Università di Perugia, I-06100 Perugia, Italy*
[61a]*INFN Sezione di Pisa, I-56127 Pisa, Italy*
[61b]*Dipartimento di Fisica, Università di Pisa, I-56127 Pisa, Italy*
[61c]*Scuola Normale Superiore di Pisa, I-56127 Pisa, Italy*
[62]*Princeton University, Princeton, New Jersey 08544, USA*
[63a]*INFN Sezione di Roma, I-00185 Roma, Italy*
[63b]*Dipartimento di Fisica, Università di Roma La Sapienza, I-00185 Roma, Italy*
[64]*Universität Rostock, D-18051 Rostock, Germany*
[65]*Rutherford Appleton Laboratory, Chilton, Didcot, Oxon, OX11 0QX, United Kingdom*
[66]*CEA, Irfu, SPP, Centre de Saclay, F-91191 Gif-sur-Yvette, France*
[67]*University of South Carolina, Columbia, South Carolina 29208, USA*
[68]*Stanford Linear Accelerator Center, Stanford, California 94309, USA*
[69]*Stanford University, Stanford, California 94305-4060, USA*
[70]*State University of New York, Albany, New York 12222, USA*
[71]*University of Tennessee, Knoxville, Tennessee 37996, USA*
[72]*University of Texas at Austin, Austin, Texas 78712, USA*

[*]Deceased.
[†]Now at Temple University, Philadelphia, PA 19122, USA.
[‡]Now at Tel Aviv University, Tel Aviv, 69978, Israel.
[§]Also with Università di Perugia, Dipartimento di Fisica, Perugia, Italy.
[‖]Also with Università di Roma La Sapienza, I-00185 Roma, Italy.
[¶]Now at University of South Alabama, Mobile, AL 36688, USA.
[**]Also with Università di Sassari, Sassari, Italy.

[73]*University of Texas at Dallas, Richardson, Texas 75083, USA*
[74a]*INFN Sezione di Torino, I-10125 Torino, Italy*
[74b]*Dipartimento di Fisica Sperimentale, Università di Torino, I-10125 Torino, Italy*
[75a]*INFN Sezione di Trieste, I-34127 Trieste, Italy*
[75b]*Dipartimento di Fisica, Università di Trieste, I-34127 Trieste, Italy*
[76]*IFIC, Universitat de Valencia-CSIC, E-46071 Valencia, Spain*
[77]*University of Victoria, Victoria, British Columbia, Canada V8W 3P6*
[78]*Department of Physics, University of Warwick, Coventry CV4 7AL, United Kingdom*
[79]*University of Wisconsin, Madison, Wisconsin 53706, USA*
(Received 28 August 2008; published 25 March 2009)

We present a study of the charmless semileptonic B-meson decays $B^+ \to \omega \ell^+ \nu$ and $B^+ \to \eta \ell^+ \nu$. The analysis is based on 3.83×10^8 $B\bar{B}$ pairs recorded at the $\Upsilon(4S)$ resonance with the *BABAR* detector. The ω mesons are reconstructed in the channel $\omega \to \pi^+ \pi^- \pi^0$ and the η mesons in the channels $\eta \to \pi^+ \pi^- \pi^0$ and $\eta \to \gamma\gamma$. We measure the branching fractions $\mathcal{B}(B^+ \to \omega \ell^+ \nu) = (1.14 \pm 0.16_{\rm stat} \pm 0.08_{\rm syst}) \times 10^{-4}$ and $\mathcal{B}(B^+ \to \eta \ell^+ \nu) = (0.31 \pm 0.06_{\rm stat} \pm 0.08_{\rm syst}) \times 10^{-4}$.

DOI: 10.1103/PhysRevD.79.052011 PACS numbers: 13.20.He

Measurements of branching fractions of charmless semileptonic B decays can be used to determine the magnitude of the Cabibbo-Kobayashi-Maskawa matrix [1] element $V_{\rm ub}$ and thus provide an important constraint on the unitarity triangle. Studies of exclusive decays allow for more stringent kinematic constraints and better background suppression than inclusive measurements. However, the predictions for exclusive decay rates depend on calculations of hadronic form factors and are thus affected by theoretical uncertainties different from those involved in inclusive decays. The description of semileptonic decays requires one or three form factors for final states with a pseudoscalar or a vector meson, respectively, if lepton masses are neglected. Currently, the most precise determination of $|V_{\rm ub}|$ with exclusive decays, both experimentally and theoretically, comes from a measurement of $B \to \pi \ell \nu$ decays [2]. It is important to study other semileptonic final states with a pseudoscalar or a vector meson to perform further tests of theoretical calculations and to improve the knowledge of the composition of charmless semileptonic decays.

In this paper, we present measurements of the branching fractions $\mathcal{B}(B^+ \to \omega \ell^+ \nu)$ and $\mathcal{B}(B^+ \to \eta \ell^+ \nu)$, where $\ell = e$, μ, and charge-conjugate modes are included implicitly. These decays have previously been studied by the CLEO [3] and *BABAR* [4,5] collaborations ($B^+ \to \eta \ell^+ \nu$) and by the Belle [6] Collaboration ($B^+ \to \omega \ell^+ \nu$). The ω meson is reconstructed in its decay to three pions ($\mathcal{B}(\omega \to \pi^+ \pi^- \pi^0) = (89.2 \pm 0.7)\%$ [7]), while for the η meson the decays to three pions and to two photons ($\mathcal{B}(\eta \to \pi^+ \pi^- \pi^0) = (22.68 \pm 0.35)\%$, $\mathcal{B}(\eta \to \gamma\gamma) = (39.39 \pm 0.24)\%$ [7]) are used. In contrast to earlier $B^+ \to \eta \ell^+ \nu$ analyses from *BABAR* [4,5], the second B meson in the event is not reconstructed; this yields a much larger candidate sample.

The results presented here are based on a data sample of 3.83×10^8 $B\bar{B}$ pairs recorded with the *BABAR* detector [8] at the PEP-II asymmetric-energy $e^+ e^-$ storage rings at the Stanford Linear Accelerator Center (SLAC). The data correspond to an integrated luminosity of 347 fb^{-1} collected at the $\Upsilon(4S)$ resonance. In addition, 35 fb^{-1} of data collected about 40 MeV below the resonance (off-resonance) are used for background studies. Simulated $B\bar{B}$ events are used to estimate signal efficiencies and shapes of signal and background distributions. Charmless semileptonic decays are simulated as a mixture of three-body decays $B \to X_u \ell \nu$ ($X_u = \pi$, η, η', ρ, ω) and have been reweighted according to the latest form-factor calculations from light-cone sum rules [9–11]. Decays to non-resonant hadronic states X_u with masses $m_{X_u} > 2m_\pi$ are simulated using the differential decay rate given in Ref. [12], which produces a smooth m_{X_u} spectrum. The GEANT4 package [13] is used to model the *BABAR* detector response.

The reconstruction of the signal decays $B^+ \to \omega \ell^+ \nu$ and $B^+ \to \eta \ell^+ \nu$ requires the identification of a charged lepton (e or μ) and the reconstruction of an ω or η meson. The two dominant sources of background are semileptonic decays with a charm meson in the final state, $B \to X_c \ell \nu$ ($X_c = D, D^*, D^{**}, D^{(*)}\pi$), and $e^+ e^- \to q\bar{q}$ ($q = u, d, s, c$) continuum events. Other backgrounds include charmless semileptonic decays that are not analyzed as signal and $B\bar{B}$ events with lepton candidates from secondary decays or from misidentification of hadrons as leptons. The center-of-mass momentum of the lepton is restricted to $|\vec{p}^*_\ell| > 1.6(1.0)$ GeV [14] for the ω (η) final state. This requirement significantly reduces those background events that have hadrons misidentified as leptons and rejects a large fraction of leptons from secondary decays or photon conversions. For the reconstruction of the ω or η meson, charged (neutral) pions are required to have a momentum in the laboratory frame above 200 (400) MeV to reduce combinatorial background. Neutral pion candidates are formed from two photons with energies above 100 MeV and an invariant mass $m_{\gamma\gamma}$ in the range $100 < m_{\gamma\gamma} < 160$ MeV. A three-pion system is accepted as an ω (η)

candidate if its invariant mass $m_{3\pi}$ is in the range $760 < m_{3\pi} < 806$ MeV for ω candidates and $540 < m_{3\pi} < 555$ MeV for η candidates. The η meson is also reconstructed via its decay into two photons, each with an energy above 50 MeV, with a two-photon invariant mass in the range $520 < m_{\gamma\gamma} < 570$ MeV. To reduce the combinatorial background, two-photon combinations are rejected as possible η candidates if either of the photons can be combined with any other photon of the event to form a system with an invariant mass close to the π^0 mass, $110 < m_{\gamma\gamma} < 160$ MeV.

Event-shape variables that are sensitive to the topological differences between jetlike continuum events and more spherical $B\bar{B}$ events are used to suppress backgrounds from $e^+e^- \to q\bar{q}$ and other QED processes. The normalized second Fox-Wolfram moment R_2 [15] is required to be less than 0.5 and a loose requirement on the second Legendre moment L_2 [16] of $L_2 < 3.0$ GeV is imposed. In addition, the event must contain at least four charged tracks.

The charged lepton is combined with an ω (η) candidate to form a so-called Y pseudoparticle candidate, whose four-momentum is defined as the sum of the corresponding lepton and hadron four-momenta. All charged tracks belonging to the Y are fit to a common vertex. This vertex fit must yield a χ^2 probability of at least 0.1%. Multiple Y candidates per event are possible and all candidates are retained. The Y multiplicity is well described by the Monte-Carlo simulation. About 96% (98%) of simulated $B^+ \to \omega\ell^+\nu$ ($B^+ \to \eta\ell^+\nu$) signal events and more than 90% of all selected data events, which include both signal and background, contain only one Y candidate.

The momentum of the candidate neutrino is calculated from the difference between the momenta of the colliding-beam particles and the vector sum of the momenta of all detected particles in the event. The energy of the candidate neutrino is obtained as the magnitude of its momentum, since this is less susceptible to bias from lost particles or additional tracks than the missing energy $E_{\rm miss}$ of the event. The magnitude of the missing-momentum vector must be at least 500 MeV. The effect of losses due to detector acceptance on the reconstruction of the neutrino candidate is reduced by requiring the missing-momentum vector in the laboratory frame to point into the polar-angle range $0.3 < \theta_{\rm miss} < 2.2$ rad. If the missing energy and momentum in the event come from a single undetected neutrino and the rest of the event is correctly reconstructed, the missing mass $m_{\rm miss}$ measured from the whole event should be compatible with zero. Because the missing-mass resolution varies linearly with the missing energy, only events with $|m^2_{\rm miss}/(2E_{\rm miss})| < 2.5$ GeV are selected.

If the Y candidate originates from a signal decay that has been correctly reconstructed, the cosine of the angle between the B meson and the Y candidate can be calculated as $\cos\theta_{BY} = (2E^*_B E^*_Y - m^2_B - m^2_Y)/(2|\vec{p}^*_B||\vec{p}^*_Y|)$. Here m_B, E^*_B, $\vec{p}^*_B$, m_Y, E^*_Y, $\vec{p}^*_Y$ refer to the masses, energies, and momenta of the B meson and the Y candidate, respectively. In the calculation of $\cos\theta_{BY}$, the B-meson energy E^*_B and momentum $\vec{p}^*_B$ are not measured event by event. Instead, $E^*_B = \sqrt{s}/2$ is given by the center-of-mass energy of the colliding-beam particles $\sqrt{s}$ and the magnitude of the B momentum is calculated as $|\vec{p}^*_B| = \sqrt{E^{*2}_B - m^2_B}$. Signal candidates are required to satisfy $-1.2 < \cos\theta_{BY} < 1.1$. This requirement was kept loose to account for the limited detector resolution and photon energy losses.

To reduce backgrounds without significant loss of signal, the momenta of the lepton $\vec{p}^*_\ell$ and of the hadron $\vec{p}^*_{\omega,\eta}$ that make up a Y candidate are restricted. For $B^+ \to \omega\ell^+\nu$, the momenta are required to satisfy $|\vec{p}^*_\omega| > 1.3$ GeV or $|\vec{p}^*_\ell| > 2.0$ GeV or $|\vec{p}^*_\omega| + |\vec{p}^*_\ell| > 2.65$ GeV. In the case of $B^+ \to \eta\ell^+\nu$, the conditions $|\vec{p}^*_\eta| > 1.3$ GeV or $|\vec{p}^*_\ell| > 2.1$ GeV or $|\vec{p}^*_\eta| + |\vec{p}^*_\ell| > 2.8$ GeV have to be fulfilled.

The kinematic consistency of the reconstructed $Y\nu$ system with a signal B decay is verified using the two variables $\Delta E = (P_B \cdot P_{\rm beam} - s/2)/\sqrt{s}$ and $m_{\rm ES} = \sqrt{(s/2 + \vec{p}_B \cdot \vec{p}_{\rm beam})^2/E^2_{\rm beam} - \vec{p}^2_B}$, where $P_{\rm beam} = (E_{\rm beam}, \vec{p}_{\rm beam})$ is the four-momentum of the colliding-beam particles and $P_B = (E_B, \vec{p}_B)$ is the B-meson four-momentum computed as the sum of the four-momenta of the Y and the ν candidates. These variables are later used to extract the signal yields in a fit to the two-dimensional ΔE vs $m_{\rm ES}$ distribution. Only candidates that fulfill the loose requirement $|\Delta E| < 0.95$ GeV and $m_{\rm ES} > 5.095$ GeV (fit region) are retained.

At this stage of the selection, the signal-to-background ratio S/B, where S and B denote the expected signal and background yields, respectively, is small. It amounts to 1.5% for $B^+ \to \omega\ell^+\nu$ and 1.8% (1.0%) for $B^+ \to \eta\ell^+\nu$ with $\eta \to \pi^+\pi^-\pi^0(\gamma\gamma)$. The signal efficiencies for the sum of decays with electrons and muons, estimated from simulation, are 2.8% for $B^+ \to \omega\ell^+\nu$ and 4.0% (9.4%) for $B^+ \to \eta\ell^+\nu$ with $\eta \to \pi^+\pi^-\pi^0(\gamma\gamma)$.

For further discrimination between the signal and the background, a multivariate selection based on neural networks [17] is used. For each of the three signal channels under study, neural networks with two hidden layers (four and two neurons, respectively) are applied consecutively to separate the signal from the two main backgrounds. A first neural network discriminates the signal against $q\bar{q}$ continuum events; a second network is used to further distinguish the signal from the $B \to X_c\ell\nu$ background. The neural-network decision is based on the following input variables: $m^2_{\rm miss}/(2E_{\rm miss})$, $\theta_{\rm miss}$, $\cos\theta_{BY}$, R_2, L_2, $\cos\Delta\theta_{\rm thrust}$, the cosine of the polar-angle difference between the thrust axes of the Y candidate and of the rest of the event, and $\cos\theta_{W\ell}$, the cosine of the lepton "helicity angle" measured in the rest frame of the virtual W (calculated using the lepton and neutrino candidates) relative to the W direction in the B

TABLE I. Signal efficiencies, $\epsilon_{\rm signal}$, and signal-to-background ratios, S/B, after the neural-network selection.

	Fit region		Signal region
	$\epsilon_{\rm signal}(\%)$	S/B	S/B
$B^+ \to \omega\ell^+\nu$	1.00	0.15	0.46
$B^+ \to \eta\ell^+\nu$, $\eta \to \pi^+\pi^-\pi^0$	1.62	0.10	0.35
$B^+ \to \eta\ell^+\nu$, $\eta \to \gamma\gamma$	4.90	0.04	0.15

rest frame. For the three-pion final states, the Dalitz amplitude, the magnitude of the vector product of the π^+ momentum and the π^- momentum in the ω/η rest frame, normalized to its maximum value, serves as an additional input variable to separate $\omega \to \pi^+\pi^-\pi^0$ and $\eta \to \pi^+\pi^-\pi^0$ decays from combinatorial background.

The training of the neural networks is done using the corresponding simulated signal and background samples for each of the three signal channels separately. Independent simulated event samples are used to validate the training. Based on Monte-Carlo simulation, the selection criterion for each of the output discriminants is chosen to maximize the quantity $S/\sqrt{S+B}$. The signal efficiencies and the S/B ratios after the neural-network selection are given in Table I for the fit region and for the signal region delimited by $-0.2 < \Delta E < 0.4$ GeV and $m_{\rm ES} > 5.255$ GeV.

For the determination of the signal branching fractions, the ΔE vs $m_{\rm ES}$ distributions of the simulated signal and backgrounds are fit to the data distribution for the three signal channels independently. The fits are based on an extended binned maximum-likelihood method [18] and take statistical fluctuations of both the data and the Monte-Carlo samples into account. The binning of the ΔE vs $m_{\rm ES}$ distributions used in the fits contains a total of 50 bins with smaller sizes in the signal region to resolve the signal shape and larger sizes in the part of the fit region outside of the signal region to determine the background normalizations from data. The shapes of the signal and background distributions are taken from simulation. The fits determine the relative fractions of the signal and some of the background samples in the data.

The free parameters of the fits are the normalizations of the signal and the $B \to X_c\ell\nu$ background, and for the $B^+ \to \omega\ell^+\nu$ channel also the overall normalization of the continuum background. The $B \to X_c\ell\nu$ normalization is left free to account for a slight discrepancy between the $B \to X_c\ell\nu$ yields in data and Monte-Carlo simulation. The relative contributions of events with electrons or muons to the continuum background have been determined using off-resonance data. Compared to the $B^+ \to \omega\ell^+\nu$ channel, the $B^+ \to \eta\ell^+\nu$ channels suffer from a larger continuum background and the fit shows larger correlations between signal and this background component. The normalization of the continuum background in the $B^+ \to \eta\ell^+\nu$ channel is therefore taken from off-resonance data and is not varied in the fit. All other background distributions, mainly other $B \to X_u\ell\nu$ decays and B decays with secondary or misidentified leptons, are fixed to their Monte-Carlo predictions. The fit procedure has been validated with simulated signal and background samples.

The resulting signal yields and branching fractions for the three signal channels are presented in Table II. The scale factors between the $B \to X_c\ell\nu$ background yields predicted by the simulation and the values determined by the fits are 1.06 ± 0.07 for $B^+ \to \omega\ell^+\nu$ and 0.96 ± 0.07 (1.12 ± 0.03) for $B^+ \to \eta\ell^+\nu$ with $\eta \to \pi^+\pi^-\pi^0$ ($\eta \to \gamma\gamma$). The correlations between the signal and the $B \to X_c\ell\nu$ parameters determined by the fits are 0.08 for $B^+ \to \omega\ell^+\nu$ and -0.60 (-0.46) for $B^+ \to \eta\ell^+\nu$ with $\eta \to \pi^+\pi^-\pi^0$ ($\eta \to \gamma\gamma$). The correlation between the signal and the continuum parameters for the $B^+ \to \omega\ell^+\nu$ channel is -0.55 and the continuum background normalization is adjusted by a factor of 0.89 ± 0.12 with respect to the normalization obtained from the off-resonance data sample. The goodness of fit is evaluated using a χ^2-based comparison of the fitted ΔE vs $m_{\rm ES}$ distributions of the simulated and data samples and is shown in Table II. In addition, the combined branching fraction for the two $B^+ \to \eta\ell^+\nu$ channels has been obtained from a fit to the sum of the ΔE vs $m_{\rm ES}$ distributions for $\eta \to \pi^+\pi^-\pi^0$ and $\eta \to \gamma\gamma$.

Figure 1 shows the projections of the fitted distributions on ΔE and $\rm m_{ES}$ for the three signal channels and the combined $B^+ \to \eta\ell^+\nu$ channel. For a better visibility of the signal, the ΔE projections are shown for $m_{\rm ES} > 5.255$ GeV and the $m_{\rm ES}$ projections are shown for $-0.2 < \Delta E < 0.4$ GeV.

The systematic errors on the measured branching fractions are listed in Table III. They are estimated by varying

TABLE II. Signal yields and corresponding branching fractions as determined by the fits for the three signal channels and the combined $B^+ \to \eta\ell^+\nu$ channel. The last row shows the χ^2 per degree of freedom.

	$B^+ \to \omega\ell^+\nu$	$B^+ \to \eta\ell^+\nu$		
		$\eta \to \pi^+\pi^-\pi^0$	$\eta \to \gamma\gamma$	Combined
$N_{\rm signal}$	802 ± 113	127 ± 42	459 ± 98	554 ± 105
$\mathcal{B}(10^{-5})$	11.4 ± 1.6	4.36 ± 1.43	3.01 ± 0.64	3.11 ± 0.59
χ^2/d.o.f.	36.0/47	59.9/48	43.2/48	49.7/48

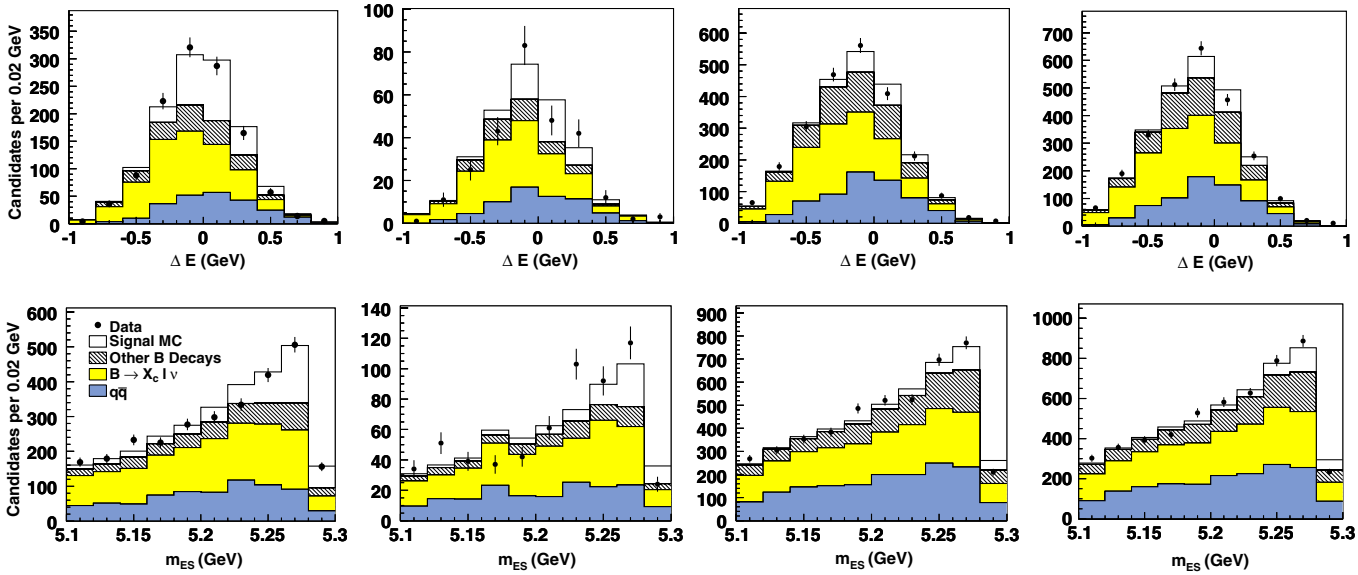

FIG. 1 (color online). Projected ΔE distributions for $m_{\rm ES} > 5.255$ GeV (top), and $m_{\rm ES}$ distributions for $-0.2 < \Delta E < 0.4$ GeV (bottom). From left to right: $B^+ \to \omega \ell^+ \nu$ channel, $B^+ \to \eta \ell^+ \nu$ channel with $\eta \to \pi^+ \pi^- \pi^0$, $B^+ \to \eta \ell^+ \nu$ channel with $\eta \to \gamma\gamma$, and combined $B^+ \to \eta \ell^+ \nu$ channel. The error bars represent the statistical uncertainties on the data. The histograms show simulated distributions for signal (white), $B \to X_c \ell \nu$ decays (light shaded/yellow), $q\bar{q}$-continuum (dark shaded/blue), and all other backgrounds (hatched) and have been summed up. The distributions of the simulated signal and $B \to X_c \ell \nu$ background (and the $q\bar{q}$ background for $B^+ \to \omega \ell^+ \nu$) have been scaled to the results of the fits.

the detection efficiencies or the parameters that impact the modeling of the signal and the background processes within their uncertainties. The complete analysis is then repeated and the differences in the resulting branching fractions are taken as the systematic errors. The total systematic error is obtained by adding in quadrature all listed contributions.

Uncertainties due to the reconstruction of charged particles and photons are evaluated by varying their reconstruction efficiencies and the energy depositions of photons in the simulation. The neutrino reconstruction is affected by background with long-lived K_L^0, which often escape detection and contribute to the measured missing momentum of the event. The uncertainty arising from K_L^0 produc-

TABLE III. Relative systematic errors of the branching fractions $\mathcal{B}(B^+ \to \omega \ell^+ \nu)$ and $\mathcal{B}(B^+ \to \eta \ell^+ \nu)$. For the $B^+ \to \eta \ell^+ \nu$ channel, the systematic errors for the three-pion and the two-photon final states as well as for the combined result are shown. The total error in each column is the sum in quadrature of all listed contributions.

Error source	$\delta\mathcal{B}(B^+ \to \omega \ell^+ \nu)(\%)$	$\delta\mathcal{B}(B^+ \to \eta \ell^+ \nu)(\%)$		
		$\eta \to \pi^+ \pi^- \pi^0$	$\eta \to \gamma\gamma$	Combined
Tracking efficiency	1.9	4.9	4.2	4.6
Photon reconstruction	2.1	1.8	9.1	8.6
K_L^0 production and interactions	2.6	4.8	3.1	1.9
Lepton identification	1.9	3.3	6.9	6.3
π^0/η identification	3.8	6.9	13.3	12.2
Neural-net input variables	0.6	0.8	5.9	6.1
D^* form factors	0.4	1.0	0.9	1.0
$\mathcal{B}(B \to X_c \ell \nu)$	2.1	5.5	7.6	8.0
$\mathcal{B}(B \to X_u \ell \nu)$	2.8	4.4	9.8	8.6
Secondary leptons	0.3	0.3	0.6	0.5
Continuum scaling	0.7	15.8	10.4	12.7
Signal form-factor(s)	1.8	5.9	0.3	1.3
$\mathcal{B}(\omega/\eta \to \pi^+ \pi^- \pi^0)$, $\mathcal{B}(\eta \to \gamma\gamma)$	0.8	1.5	0.6	1.2
$N_{B\bar{B}}$	1.1	1.1	1.1	1.1
f_{+-}/f_{00}	1.2	1.4	0.9	1.0
Total systematic error	7.2	21.1	25.2	25.1

tion and interactions is estimated by varying their production rate as well as their detection efficiency and energy deposition in the simulation. For lepton identification, relative uncertainties of 1.4% and 3% are used for electrons and muons, respectively. A 3% uncertainty is assigned to the $\pi^0/\eta \to \gamma\gamma$ reconstruction efficiency.

The uncertainty due to the $B \to X_c \ell \nu$ background is evaluated by varying the $B \to D/D^*/D^{**}\ell\nu$ branching fractions [7] and the $B \to D^*$ form factors [19]. Prior to the neural-network selection, the background level is high and discrepancies between data and Monte-Carlo distributions are observed at roughly the 10% level for some of the neural-network input variables. To estimate the effect of these discrepancies on the measured branching fractions, the dominant background component ($B \to X_c \ell \nu$) is reweighted to match the data. The weights are determined from a $B \to X_c \ell \nu$-enhanced sample which is obtained by selecting only events that are otherwise rejected by the $B \to X_c \ell \nu$ neural-network selection and keeping all other selection criteria unchanged.

For the $B \to X_u \ell \nu$ background, the branching fractions of the exclusive decays that are not analyzed as signal are varied within their uncertainties [20]. The nonresonant part is varied within the range allowed by the uncertainty of the total $B \to X_u \ell \nu$ branching fraction [20]. The uncertainty due to the normalization of the continuum background has been determined with off-resonance data for events with electrons or muons separately. Since the overall normalization of the continuum background is adjusted for $B^+ \to \omega \ell^+ \nu$ in the fit, the resulting error in this channel is smaller than for the $B^+ \to \eta \ell^+ \nu$ channels. For the normalization of secondary-lepton background, an uncertainty of 6–8%, depending on the signal channel, has been estimated from a detailed study of the composition of this background.

Uncertainties in the modeling of signal decays due to the imperfect knowledge of the form factors affect the shapes of kinematic spectra and thus the acceptances of signal decays. The errors on the measured branching fractions are estimated by varying the parameters of the form-factor calculations within their uncertainties [10,11].

The branching fractions of the decays $\omega/\eta \to \pi^+\pi^-\pi^0$ and $\eta \to \gamma\gamma$ are also varied within their uncertainties [7]. The uncertainty on the number of produced B mesons is 1.1% [21]. The uncertainty on the ratio of the $\Upsilon(4S) \to B^+B^-$ and $\Upsilon(4S) \to B^0\bar{B}^0$ branching fractions, $f_{+-}/f_{00} = 1.065 \pm 0.026$ [20], is taken into account.

The total systematic errors on the measured branching fractions are 7.2% and 25.1% for the $B^+ \to \omega \ell^+ \nu$ and the combined $B^+ \to \eta \ell^+ \nu$ channels, respectively.

In summary, we have measured the branching fractions of $B^+ \to \omega \ell^+ \nu$ and $B^+ \to \eta \ell^+ \nu$ decays to be

$$\begin{aligned} \mathcal{B}(B^+ \to \omega \ell^+ \nu) &= (1.14 \pm 0.16 \pm 0.08) \times 10^{-4}, \\ \mathcal{B}(B^+ \to \eta \ell^+ \nu) &= (0.31 \pm 0.06 \pm 0.08) \times 10^{-4}, \end{aligned} \tag{1}$$

where the errors are statistical (data and simulation) and systematic, respectively.

The $B^+ \to \eta \ell^+ \nu$ and $B^+ \to \omega \ell^+ \nu$ measurements presented here significantly improve the current knowledge of these decays. The $B^+ \to \eta \ell^+ \nu$ result is compatible with an earlier measurement by *BABAR* [5] based on events tagged by a semileptonic decay of the second B meson, $\mathcal{B}(B^+ \to \eta \ell^+ \nu) = (0.64 \pm 0.20_{\text{stat}} \pm 0.03_{\text{syst}}) \times 10^{-4}$. The two analyses are statistically independent and complement each other. The analysis presented here is statistically more precise but has larger systematic uncertainties, as expected for an untagged measurement. We combine the two *BABAR* results and obtain $\mathcal{B}(B^+ \to \eta \ell^+ \nu) = (0.37 \pm 0.06_{\text{stat}} \pm 0.07_{\text{syst}}) \times 10^{-4}$. The $B^+ \to \omega \ell^+ \nu$ branching-fraction measurement is the first with a significance of more than 5 standard deviations. It represents an improvement by a factor of 3 over the only earlier measurement by Belle [6]. The improved measurements of $B^+ \to \omega \ell^+ \nu$ and $B^+ \to \eta \ell^+ \nu$ decays are important ingredients to the determination of the composition of the inclusive charmless semileptonic decay rate. The size of the data samples is not yet sufficient to perform a measurement in intervals of the momentum transfer q^2 of the decay, which would be necessary to determine $|V_{ub}|$ with an adequate precision.

We are grateful for the excellent luminosity and machine conditions provided by our PEP-II colleagues, and for the substantial dedicated effort from the computing organizations that support *BABAR*. The collaborating institutions wish to thank SLAC for its support and kind hospitality. This work is supported by DOE and NSF (USA), NSERC (Canada), IHEP (China), CEA and CNRS-IN2P3 (France), BMBF and DFG (Germany), INFN (Italy), FOM (The Netherlands), NFR (Norway), MIST (Russia), and PPARC (United Kingdom). Individuals have received support from CONACyT (Mexico), A. P. Sloan Foundation, Research Corporation, and Alexander von Humboldt Foundation.

[1] M. Kobayahi and T. Maskawa, Prog. Theor. Phys. **49**, 652 (1973).

[2] B. Aubert *et al.* (*BABAR* Collaboration), Phys. Rev. Lett. **98**, 091801 (2007).

[3] S. B. Athar *et al.* (CLEO Collaboration), Phys. Rev. D **68**, 072003 (2003); D. M. Asner *et al.* (CLEO Collaboration), Phys. Rev. D **76**, 012007 (2007).
[4] B. Aubert *et al.* (*BABAR* Collaboration), arXiv:hep-ex/0607066v1 (contribution to ICHEP, Moscow, 2006).
[5] B. Aubert *et al.* (*BABAR* Collaboration), Phys. Rev. Lett. **101**, 081801 (2008).
[6] C. Schwanda *et al.* (Belle Collaboration), Phys. Rev. Lett. **93**, 131803 (2004).
[7] W.-M. Yao *et al.* (Particle Data Group), J. Phys. G **33**, 1 (2006) and 2007 partial update for the 2008 edition.
[8] B. Aubert *et al.* (*BABAR* Collaboration), Nucl. Instrum. Methods Phys. Res., Sect. A **479**, 1 (2002).
[9] P. Ball and R. Zwicky, Phys. Rev. D **71**, 014015 (2005).
[10] P. Ball and R. Zwicky, Phys. Rev. D **71**, 014029 (2005).
[11] P. Ball and G. W. Jones, J. High Energy Phys. 08 (2007) 025.
[12] F. De Fazio and M. Neubert, J. High Energy Phys. 06 (1999) 017.
[13] S. Agostinelli *et al.* (GEANT4 Collaboration), Nucl. Instrum. Methods Phys. Res., Sect. A **506**, 250 (2003).
[14] All variables denoted with a star (e.g. p^*) are given in the $\Upsilon(4S)$ rest frame; all others are in the laboratory frame except if differently specified.
[15] G. C. Fox and S. Wolfram, Phys. Rev. Lett. **41**, 1581 (1978).
[16] $L_2 = \sum_i |\vec{p}_i^*| \cos^2(\theta_i^*)$, where the sum is over all tracks in the event not used to form the Y candidate and $\vec{p}_i^*$ and θ_i^* are their momenta and angles with respect to the thrust axis of the Y candidate, respectively.
[17] A. Höcker *et al.*, Proc. Sci. ACAT2007 (2007) 040 [arXiv: physics/0703039v4].
[18] R. J. Barlow and C. Beeston, Comput. Phys. Commun. **77**, 219 (1993).
[19] B. Aubert *et al.* (*BABAR* Collaboration), Phys. Rev. D **77**, 032002 (2008).
[20] E. Barberio *et al.* (Heavy Flavor Averaging Group), arXiv:0808.1297.
[21] B. Aubert *et al.* (*BABAR* Collaboration), Phys. Rev. D **67**, 032002 (2003).